Effects of minor Cu and Mg additions on microstructure and material properties of 8xxx aluminum conductor alloys

Lei Pan[1], Kun Liu[1], Francis Breton[2] and X.-Grant Chen[1,*]

[1] *Department of Applied Sciences, Université of Québec at Chicoutimi*

Saguenay, QC, G7H 2B1, Canada

[2] *Arvida Research and Development Centre, Rio Tinto, Saguenay, QC, G7S 4K8, Canada,*

* Corresponding author:

X.-Grant Chen, Tel.: 1-418-545 5011 ext. 2603; Fax: 1-418-545 5012;

E-mail: xgrant_chen@uqac.ca

Effects of minor Cu and Mg additions on microstructure and material properties of 8xxx aluminum conductor alloys

Abstract

The effects of minor Cu (0−0.29 wt.%) and Mg (0−0.1 wt.%) additions on the microstructure, electrical conductivity, mechanical and creep properties of 8xxx aluminum conductor alloys were studied. The microstructure evolution was investigated using an optical microscope and the electron backscattered diffraction technique. The creep property was characterized by the primary creep strain and the minimum creep rate during creep deformation. The results demonstrated that additions of minor Cu and Mg reasonably improved the ultimate tensile strength but slightly reduced electrical conductivity. The addition of Cu remarkably decreased the primary creep strain but had a negligible effect on the minimum creep rate, leading to a beneficial effect on the short-term creep resistance but no advantage to the creep resistance under the long-term creep process. The minor addition of Mg greatly reduces both primary creep strain and minimum creep rate, resulting in a significant and effective improvement in the creep resistance.

1. Introduction

As the economy has developed in the past decades, the demand for electrical conductor materials has been significantly increasing.[1,2] The 8xxx aluminum conductor alloys offer significant advantages, such as low density, high electrical conductivity to weight ratio and low

cost over copper conductors. These materials are progressively replacing copper conductor alloy in overhead transmission and electrical distribution within buildings.[1,3] For a wider application of aluminum conductors, it is necessary to satisfy the overall requirements of materials properties in the electrical industry, notably the electrical conductivity, tensile strength and creep resistance.[2,4] Consequently, considerable efforts have been devoted to develop aluminum conductor alloys with higher comprehensive properties.[4,5]

Adding minor alloying elements in 8xxx aluminum conductor alloys, such as Cu and Mg, is often considered an efficient and economical way to obtain better comprehensive properties.[4-6] Alloying of commercially pure aluminum alloy may create solid solutions or individual phases that greatly improve tensile strength due to solid solution strengthening and precipitation strengthening.[7,8] However, the electrical conductivity may decrease because of the enhanced scattering of free electrons at solute atoms and precipitates.[9] For electrical applications, it is a challenge to find a favorable combination of high electrical conductivity with enhanced mechanical properties in the design and development of alloys.

In addition, creep resistance is one of the most important properties required in aluminum conductor alloys.[2] Previous investigations have demonstrated that the creep properties of aluminum alloys can be significantly affected by alloying elements.[6,10-15] In general, alloying in pure aluminum increases the creep resistance by decreasing grain boundary mobility, impeding dislocation movement and accelerating dislocation multiplication.[10,11,13] Several researchers have

investigated the effect of Cu addition on creep properties in aluminum alloys; however, the results appear to be somewhat inconsistent. Chaudhury *et al*.[10] reported that an Al−2 wt.% Cu alloy exhibited higher creep property compared with pure aluminum due to the segregation of Cu atoms to moving dislocations. Reynolds *et al*.[14] investigated the creep behavior of Al alloys containing Cu (0.64−1.72 wt.%) and found that the addition of Cu had a negligible effect on the creep properties. Kato[15] studied the sliding in bicrystals of Al−Cu solid solutions and noted that small Cu addition decreases the creep property. Conversely, several studies suggested that Mg addition in aluminum could enhance the creep property at relatively high temperatures (> 0.5 T_m, where T_m is the absolute melting point of the alloy).[6,11] For instance, Du *et al*.[11] reported that Mg atoms could increase the creep property by increasing the sliding threshold of grain boundaries by forming immobile Mg−Al clusters. Marquis *et al*.[6] reported that Mg addition could strengthen the creep property of Al−2 wt.% Mg−0.2 wt.% Sc alloy at 300 ºC by increasing the threshold stress. To the best of the author's knowledge, few investigations have been conducted on the effect of Cu and Mg on the creep properties of aluminum conductor alloys at relatively low temperatures (≤ 0.4 T_m), which are the normal service temperature range for most aluminum conductor alloys.

In the present study, 8xxx aluminum alloys with three Fe levels were alloyed with different but small amounts of Cu and Mg. The evolution of electrical conductivity and tensile strength as a function of Cu, Mg and Fe content was explored and quantitatively analyzed. The effect of Cu and Mg on the creep properties at 100 ºC was systematically investigated.

2. Experimental

The materials used in the experiments were 8xxx aluminum alloys with three fixed Fe levels (Al−0.3Fe, Al−0.5Fe and Al−0.7Fe base alloys) alloyed with various Cu and Mg concentrations. Because of a remarkable decrease of electrical conductivity by solute atoms in aluminum alloys, only small amounts Cu and Mg were added in the present work to keep a favorable combination of high mechanical strength with reasonable electrical conductivity. The additions of 0.18% and 0.29% Cu were made to Al−0.3Fe, Al−0.5Fe and Al−0.7Fe base alloys, and further addition of 0.025%, 0.05% and 0.1% Mg were made to Al−0.3Fe−0.18Cu, Al−0.5Fe−0.18Cu and Al−0.7Fe−0.18Cu alloys, respectively. A total of 18 alloys with various Cu, Mg and Fe contents were batched in an electrical resistance furnace and cast in the form of round billets with 4 inch diameters by a direct chill (DC) cast unit. Their chemical compositions are shown in Table I. All the rod samples with 9.5 mm in diameter, which are equivalent to the industrial 9.5 mm supply rods for drawn wire, were produced by hot extrusion from the DC cast billets.

Table I Chemical compositions of the experimental alloys (wt. %)

Alloys	Fe	Cu	Mg	Si	Mn	Cr	Zn	Al
Al-0.3Fe (L00)	0.30	**0.01**	0.001	0.025	0.002	0.001	0.012	Bal.
Al-0.3Fe-0.18Cu (L20)	0.30	**0.18**	0.001	0.023	0.003	0.001	0.002	Bal.
Al-0.3Fe-0.29Cu (L30)	0.30	**0.29**	0.000	0.033	0.001	0.001	0.012	Bal.
Al-0.3Fe-0.18Cu-0.03Mg (L23)	0.30	0.18	**0.025**	0.031	0.002	0.001	0.012	Bal.
Al-0.3Fe-0.18Cu-0.05Mg (L25)	0.30	0.19	**0.052**	0.038	0.003	0.001	0.002	Bal.
Al-0.3Fe-0.18Cu-0.1Mg (L210)	0.30	0.18	**0.100**	0.049	0.002	0.001	0.012	Bal.
Al-0.5Fe (M00)	0.46	**0.01**	0.001	0.046	0.002	0.001	0.012	Bal.

Al-0.5Fe-0.18Cu (M20)	0.50	**0.18**	0.001	0.027	0.004	0.001	0.002	Bal.
Al-0.5Fe-0.29Cu (M30)	0.47	**0.29**	0.000	0.023	0.002	0.001	0.003	Bal.
Al-0.5Fe-0.18Cu-0.03Mg (M23)	0.46	0.18	**0.026**	0.051	0.002	0.001	0.013	Bal.
Al-0.5Fe-0.18Cu-0.05Mg (M25)	0.44	0.17	**0.055**	0.021	0.001	0.001	0.002	Bal.
Al-0.5Fe-0.18Cu-0.1Mg (M210)	0.47	0.18	**0.100**	0.049	0.002	0.001	0.012	Bal.
Al-0.7Fe (H00)	0.70	**0.01**	0.001	0.023	0.002	0.001	0.013	Bal.
Al-0.7Fe-0.18Cu (H20)	0.70	**0.19**	0.001	0.042	0.003	0.001	0.016	Bal.
Al-0.7Fe-0.29Cu (H30)	0.71	**0.29**	0.000	0.032	0.003	0.001	0.002	Bal.
Al-0.7Fe-0.18Cu-0.03Mg (H23)	0.69	0.18	**0.027**	0.052	0.002	0.001	0.013	Bal.
Al-0.7Fe0.18-Cu-0.05Mg (H25)	0.70	0.18	**0.056**	0.042	0.003	0.001	0.012	Bal.
Al-0.7Fe-0.18Cu-0.1Mg (H210)	0.72	0.18	**0.100**	0.051	0.002	0.001	0.013	Bal.

The electrical conductivity measurements were directly conducted on 200 mm long samples of 9.5 mm wire using a Megger DLRO10HD resistance ohmmeter. Tensile testing was carried out on cylindrical specimens (9.5 mm in diameter and 250 mm in length) according to the ASTM B557 standard at room temperature. The compression creep tests were performed at 100 ºC for 100 hours under a constant load of 69 MPa using cylindrical specimens (9.5 mm in diameter and 19 mm in length). To confirm the reliability of the results, three tests were repeated for each condition.

For microstructure examination, the extruded rods were first cut to 20 mm in length, and then sectioned longitudinally along the centerline. All of the samples were polished and etched with Keller's solution for 10 s and were later observed using an optical microscope (OM), scanning electron microscope (SEM) and electron backscattered diffraction (EBSD) technique. The automated EBSD maps were conducted on the deformed structure with a 0.2 μm step size using HKL Channel 5 software for substructure analysis. The linear intercept method was used to

measure the subgrain size of alloys with different alloying content.[16] To ensure statistical reliability, more than 200 subgrains were measured in each sample.

3. Results and Discussion

3.1 Microstructure evolution

Fig. 1 shows optical micrographs of some typical alloys with different compositions after extrusion. Due to a very low solubility of Fe in the aluminum matrix, almost all of the Fe precipitated out in the form of Fe-containing intermetallic particles in the cast microstructure. After hot extrusion, the Fe-containing intermetallic particles were broken down to a number of fine intermetallic dispersion particles. For all of the alloys, the fine intermetallic particles, which were confirmed as Al_mFe in our previous work,[17] were uniformly distributed along the extrusion direction in the aluminum matrix. By increasing Fe from 0.3 to 0.7% in the three base alloys, the volume fraction of Fe-containing intermetallic particles increased from 1.8% in Al−0.3Fe to 3.2% in Al−0.5Fe and further to 4.4% in Al−0.7Fe alloys. The sizes of the Fe-containing intermetallic particles were very similar for all the alloys studied, with an average size of 0.38 μm. When adding Cu and Mg in the three base alloys, the volume fraction of intermetallic particles was found to remain almost unchanged compared to the corresponded base alloys, which are shown in Figs. 1(a) and (b) for the addition of 0.29% Cu and in Figs. 1(c) and (d) for the combined addition of 0.18% Cu and 0.1% Mg. This result can be attributed to the higher solid solubility of Cu and Mg in

aluminum, which is approximately 0.4% and 1.7% at room temperature, respectively.[18] Therefore, all of the additions of Cu up to 0.29% and Mg up to 0.1% in this study are expected to remain in the solid solution after extrusion.

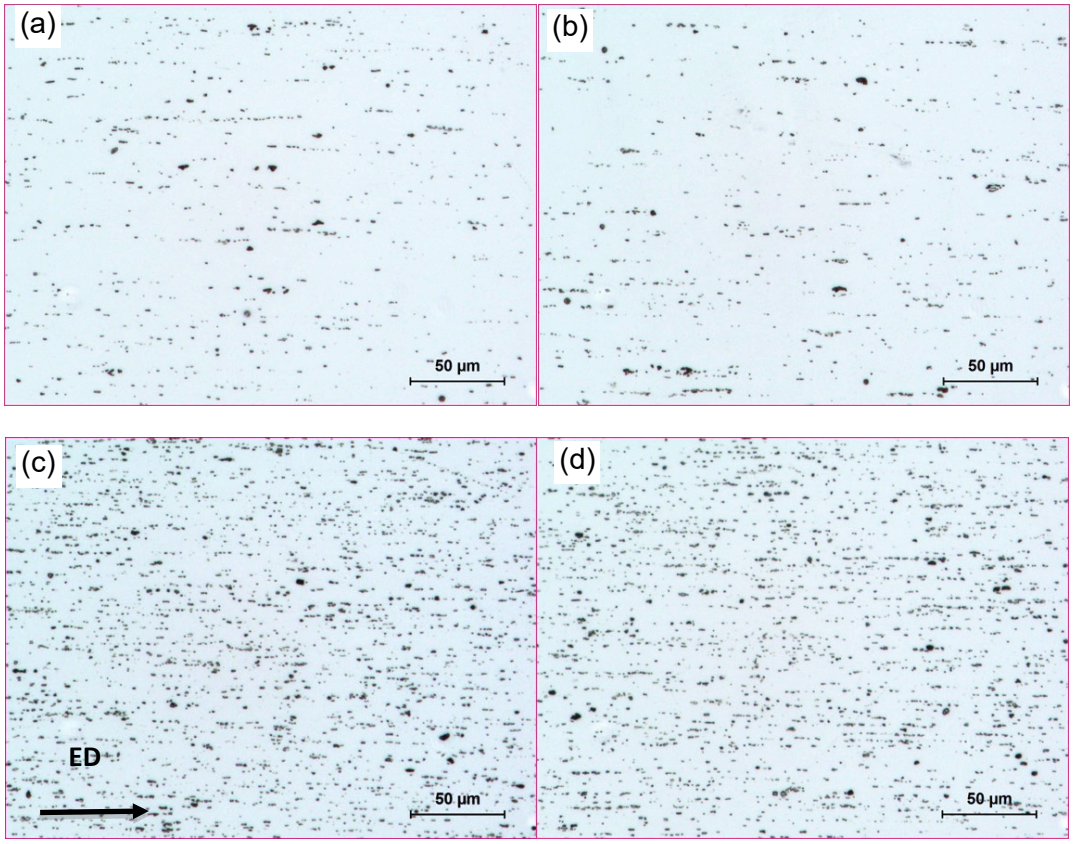

Fig. 1 Optical micrographs showing the particles distribution of the alloys: (a) Al−0.3Fe, (b) Al−0.3Fe−0.29Cu, (c) Al−0.7Fe, and (d) Al−0.7Fe−0.18Cu−0.1Mg, showing fine Fe-containing intermetallic particles distributed along the extrusion direction (ED).

To understand the microstructure evolution with the additions of Cu and Mg in 8xxx aluminum alloys, EBSD orientation maps of the same typical alloy samples as in Fig. 1 were

examined, and the results are shown in Fig. 2. It can be observed that all of the extruded alloys showed a characteristic recovered structure, in which a large amount of low-angle boundaries with misorientation angles between of 1° and 5° were observed. In addition, the substructures were organized, and large well-defined subgrains (arrowed in Fig. 2) were formed along the elongated grains with neatly arranged boundaries of 1−15°.

Though the recovered structure is present in all experimental alloys, there are differences in subgrain size due to the additions of Cu and Mg (Fig. 3). It was observed that by increasing the Cu content to 0.29%, the average subgrain size slightly decreased from 4.5 to 3.8 μm in Al−0.3Fe-Cu, from 3.7 to 3.3 μm in Al−0.5Fe−Cu and from 3.2 to 2.7 μm in Al−0.7Fe−Cu (Fig. 3(a)), respectively. However, the addition of Mg (0.025−0.1%) in all three base alloys showed a negligible change on subgrain size. As shown in Fig. 3(b), with increasing Mg content, the subgrain size kept almost constant in the three corresponding base alloys. This can be attributed to the various diffusion behaviors of Cu and Mg. Firstly, Cu solutes in aluminum solution have a lower diffusion rate than Al self-diffusion, which would strongly hinder the dislocation movement at the subgrain boundaries and enhance dislocation multiplication, leading to the retardation of the dynamic recovery.[19,20] However, the diffusion rate of Mg is very close to the Al self-diffusion rate, resulting in little effect on the dynamic recovery. As a result, the subgrain size decreased with increasing Cu level, while the Mg addition exhibited no change on subgrain size.

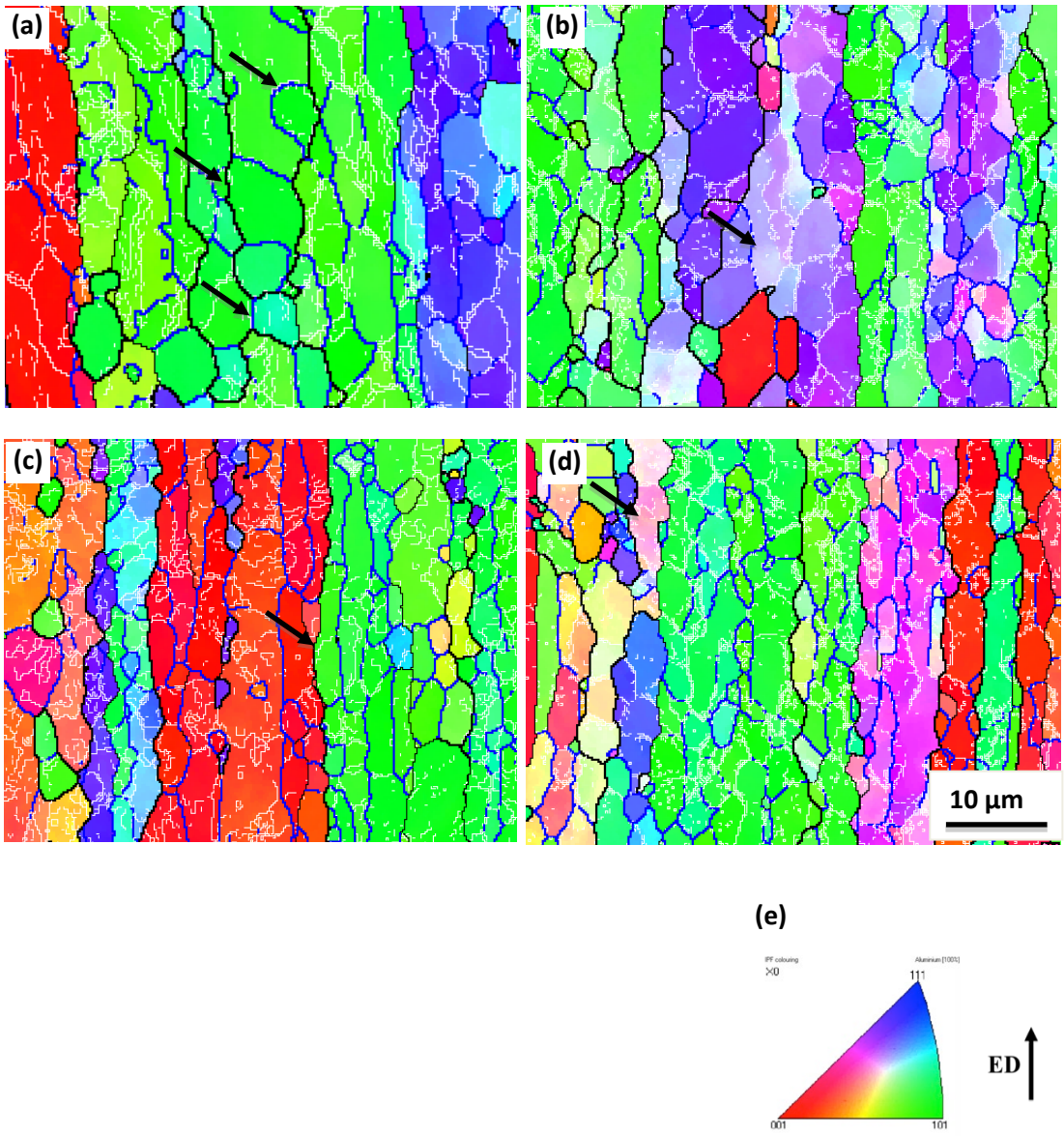

Fig. 2 Orientation image mapping showing the extruded microstructure of the alloys: (a) Al−0.3Fe, (b) Al−0.3Fe−0.29Cu, (c) Al−0.7Fe, (d) Al−0.7Fe−0.18Cu−0.1Mg and (e) inversed pole figure coloring and extrusion direction (ED). Boundary misorientation indicated as follows: white lines 1−5°, blue lines: 5−15°, thin black lines: 15−30°, and thick black lines > 30°.

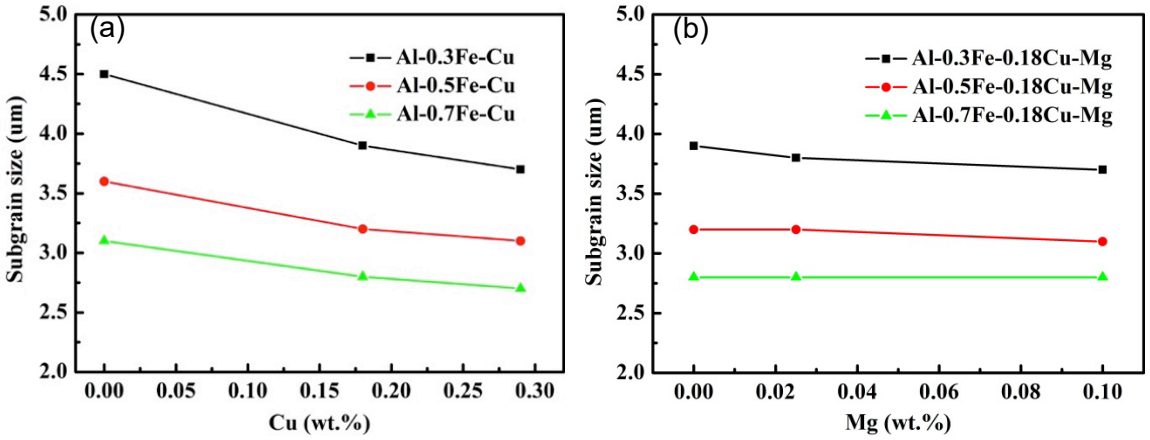

Fig. 3 The evolution of subgrain size with an increase of (a) Cu and (b) Mg content.

3.2 Electrical conductivity and tensile strength

Fig. 4 shows the evolution of the electrical conductivity (EC) with different amounts of Cu and Mg. It can be observed that EC slightly decreases with increasing Cu and Mg due to enhanced scattering of free electrons on Cu and Mg solutes in aluminum.[9] With increasing Cu content from 0 to 2.9%, EC decreased from 62.4% to 60.5%IACS in Al−0.3Fe alloy and from 60.9% to 59.1%IACS in Al−0.7Fe alloy (Fig. 4(a)). With increasing Mg content from 0% to 0.1%, EC decreases from 61.1% to 60.2%IACS in Al−0.3Fe−0.18Cu alloy and from 59.7% to 58.8%IACS in Al−0.7Fe−0.18Cu alloy (Fig. 4(b)).

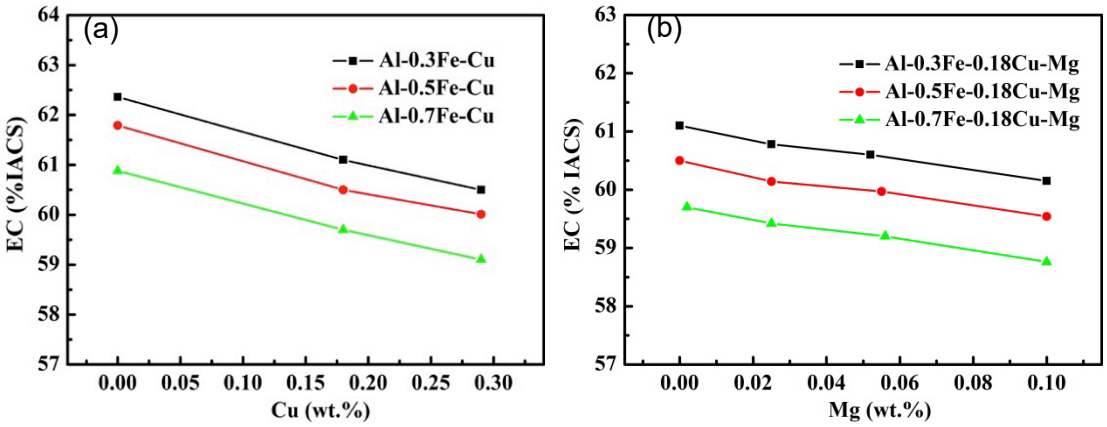

Fig. 4 Influence of alloying elements on electrical conductivity: (a) Cu and (b) Mg.

In the present work, Matthiessen's law was adapted to establish the relationship of the EC with chemical composition as follows:[21]

$$\frac{1}{EC} = \rho_b + \sum_i \rho_i C_i + \rho_P f_P \quad \cdots\cdots\cdots\cdots\cdots\cdots\cdots\cdots \text{(Eq. 1)}$$

where EC is the electrical conductivity; ρ_b is resistivity of the base alloy; $\sum_i \rho_i C_i$ is the sum of the resistivity contributions from the various solutes, *i.e.,* ρ_i is the resistivity parameter and C_i is the concentration of the i^{th} solute; ρ_p is the resistivity parameter of the particles; and f_p is the particle volume fraction. In the present study, due to a very low solubility of Fe in aluminum, it can be assumed that almost all of the Fe precipitated out into Fe-containing intermetallic particles and the amount of Fe solutes is negligible. The volume fraction of Fe-containing intermetallic particles (f_p in Eq. 1) has a linear relation with Fe concentration (C_{Fe}). [18] Hence, the particle contribution $\rho_p f_p$ in Eq. 1 can be substituted by $\rho'_{Fe} C_{Fe}$, in which ρ'_{Fe} is treated as the resistance parameter of Fe

alloying element. As all of the alloys had similar particles size, consequently, Eq. 1 in the present work can be transformed to:

$$\frac{1}{EC} = \rho_b + \rho_{Cu}C_{Cu} + \rho_{Mg}C_{Mg} + \rho'_{Fe}C_{Fe} \quad \text{(Eq. 2)}$$

where EC is in the units of %IACS; ρ_{Cu}, ρ_{Mg} and ρ'_{Fe} are the resistivity parameters of Cu, Mg and Fe alloying elements; and C_{Cu}, C_{Mg} and C_{Fe} are the concentrations in wt.%. Based on the results from Fig. 4, the values of all resistivity parameters (ρ) can be obtained using the multiple linear regression. Therefore, an empirical expression can be obtained to predict the electrical conductivity as a function of alloying element content:

$$\frac{1}{EC} = 0.01575 + 0.00174C_{Cu} + 0.00289C_{Mg} + 0.00096C_{Fe} \quad \text{(Eq. 3)}$$

The calculated values of the electrical conductivity versus the measured values with different Cu and Mg content in three base alloys are plotted in Fig. 5. As demonstrated, there is excellent agreement between the calculated and experimental results. Furthermore, to evaluate the accuracy of equation 3, the error between the calculated $EC(C)$ and the measured $EC(M)$ can be expressed as follows:

$$Error\% = \left|\frac{EC(C) - EC(M)}{EC(M)}\right| 100 \quad \text{(Eq. 4)}$$

The mean error for the 8xxx alloys with Cu contents ranging from 0% to 0.29% and Mg contents ranging from 0% to 0.1% was determined to be 0.13%, confirming the excellent

agreement between the calculated and measured EC. Therefore, Eq. 3 offers a very useful tool to predict the electrical conductivity as a function of alloying element (Cu, Mg and Fe) in 8xxx aluminum alloys.

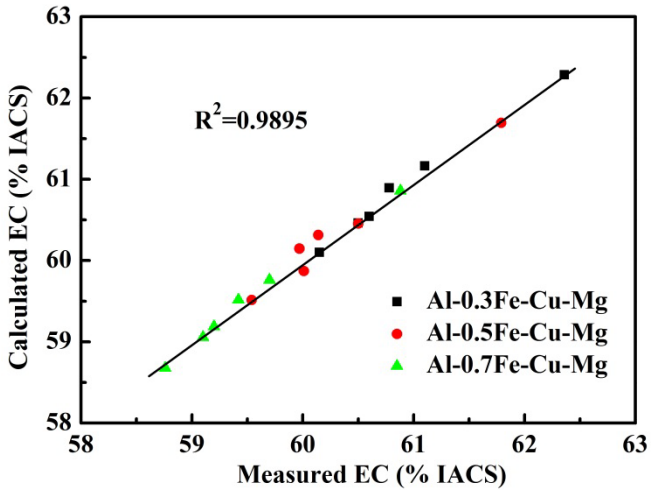

Fig. 5 Correlation between calculated and experimentally measured EC.

The ultimate tensile strength (UTS) of the alloys was evaluated with different compositions, and the results are shown in Fig. 6. It was found that the UTS showed a nearly linear relationship with Cu, Mg and Fe content and the values moderately increased with increasing Cu and Mg concentrations due to the multi-strengthening mechanisms, such as solid solution strengthening, substructure strengthening as well as the interaction between solution atoms. [7] The results reveal a beneficial effect of Cu and Mg on the mechanical properties. The overall strength σ (UTS) of the alloys can be expressed by an empirical equation in the form: [6, 8]

$$\sigma\,(\mathrm{UTS}) = \sigma_b + H_{Cu}C_{Cu} + H_{Mg}C_{Mg} + H_{Fe}C_{Fe} \quad \cdots\cdots\cdots\cdots\cdots\cdots \quad \text{(Eq. 5)}$$

where σ_b is strength of the base alloy in the units of MPa; H_{Cu}, $H_{Mg,}$ and H_{Fe} are the strengthening parameters of Cu, Mg and Fe; and C_{Cu}, C_{Mg} and C_{Fe} are the concentrations in wt.%. By using the multiple linear regression method, the values of σ_b and strengthening parameters (H) can be determined from the results of Fig. 6. Next, the following equation can be used to describe the UTS as a function of alloying element content:

$$UTS = 75.6 + 51.1C_{Cu} + 66.7C_{Mg} + 71.0C_{Fe} \quad \cdots\cdots\cdots\cdots\cdots\cdots \text{(Eq. 6)}$$

The calculated values of the UTS versus the measured values for 8xxx alloys with various Cu, Mg and Fe content in different base alloys are plotted in Fig. 7, which demonstrates a good agreement between the calculated and experimentally measured results. The mean error between the calculated and measured values for the 8xxx alloys was determined to be 1.0%, which confirms the accuracy of Eq. 6. Therefore, the obtained equation could be used to predict the UTS with various Cu, Mg and Fe additions in 8xxx aluminum alloys.

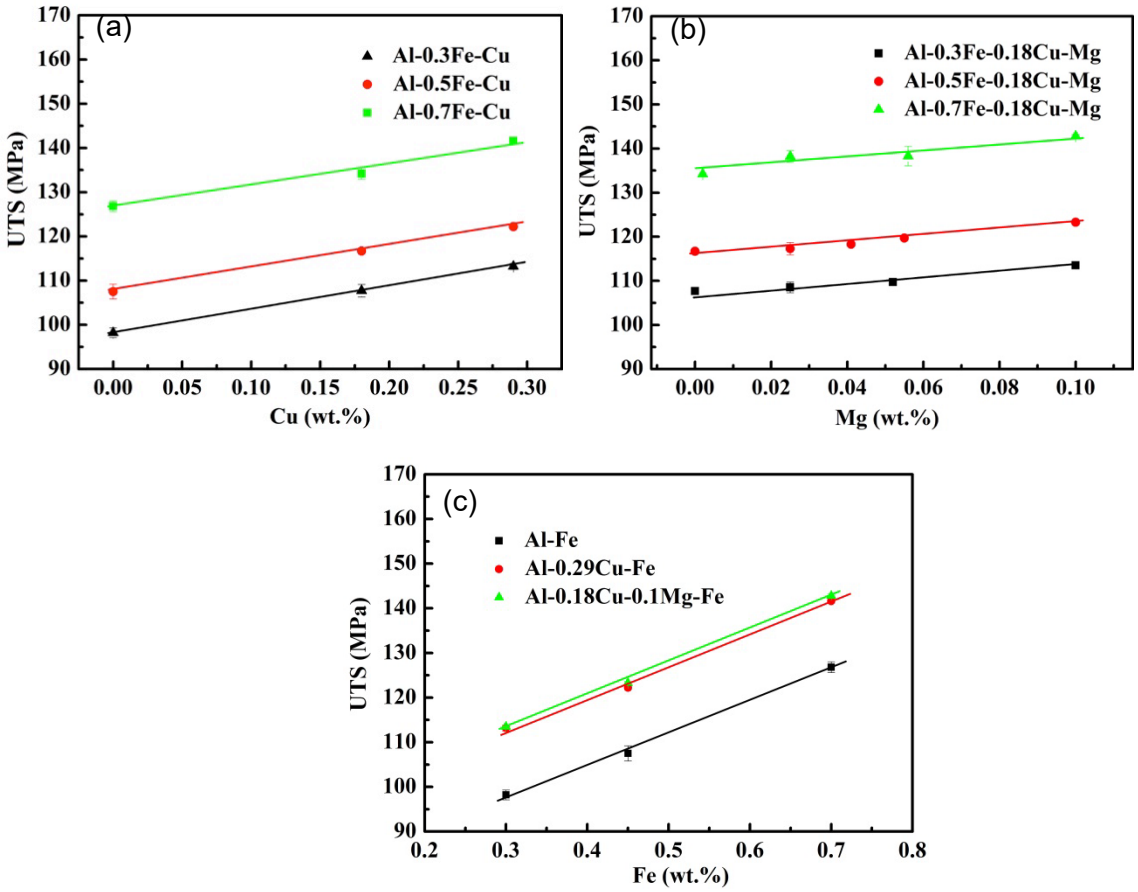

Fig. 6 Influence of individual alloying elements on UTS: (a) Cu, (b) Mg and (c) Fe with a linear relationship.

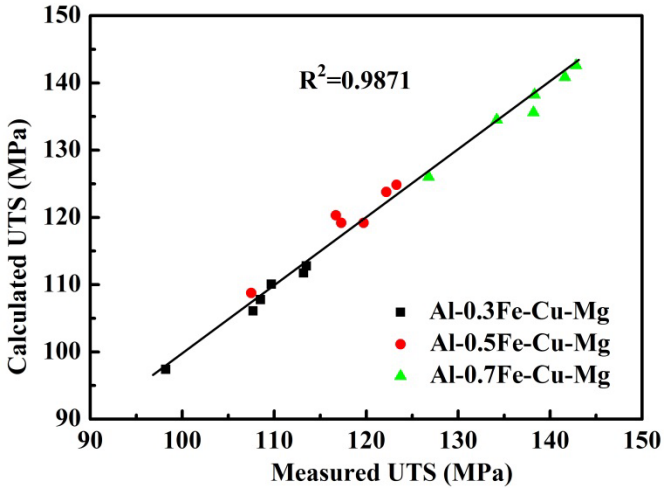

Fig. 7 Correlation between calculated and experimentally measured UTS.

In brief, the changes of properties (EC, UTS, etc.) are greatly related to the microstructure resulted from the various Fe, Cu and Mg contents. As shown in Fig. 1, the volume fraction of Fe-containing intermetallic particles increases with increasing Fe contents, which is the principle reason for the decrease of EC and the increase of UTS. The substructure derived from the addition of Cu and Mg (Fig. 2) also induces the change of UTS. In addition, Cu and Mg in the solid solution make a remarkable contribution to increase UTS and decrease EC.

For aluminum conductor alloys, high EC with enhanced UTS are most desirable in 8xxx aluminum alloys. However, high EC and high UTS are usually contradictory because of the metallurgical nature of both properties. In an attempt to have a tool for alloy development and design, the EC and UTS profile of the alloys with different Cu and Mg additions in Al−0.3Fe, Al−0.5Fe and Al−0.7Fe base alloys are plotted in Fig. 8. This figure can be divided into three regions with different combinations of EC and UTS. It is evident that there is always a trade-off between EC and UTS. Region I has high UTS but low EC while region III has high EC but low UTS. Region II in the middle has balanced EC and UTS. In the present study, both 0.3Fe (L00) and 0.5Fe (M00) alloys have higher EC but lower UTS (region III) compared to 0.7Fe (H00) alloy (region II). With the additions of Cu and Mg (see black and red arrows), the 0.3Fe and 0.5Fe alloys move to the region II with more balanced EC and UTS. For example, the 0.5Fe alloys with Cu and Mg additions could have enhanced values of UTS at the expense of EC. It is also evident that the

0.7 alloys with Cu and Mg additions tend to move from the region II to the region I, which have higher UTS but relatively lower EC. By adjusting Fe, Cu and Mg alloying elements, different combinations of EC and UTS could be obtained to fulfill various design requirements for specific applications.

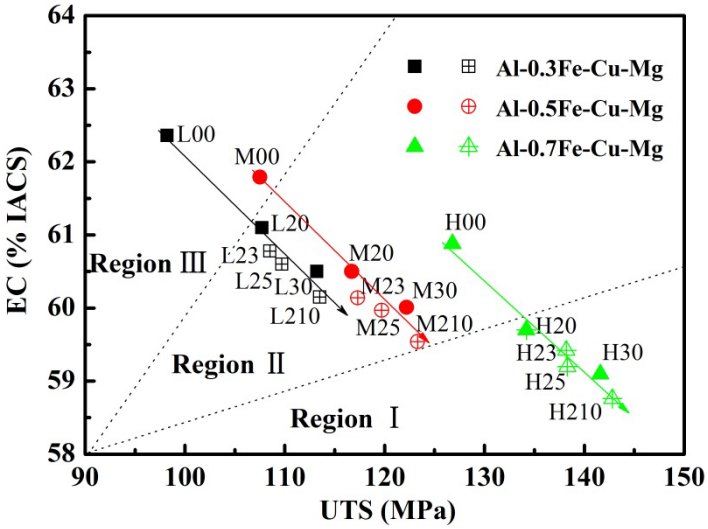

Fig. 8 EC and UTS profile of the alloys with different Cu and Mg addition. Arrows show the increasing Cu and Mg additions to their corresponding regions.

3.3 Effects of Cu and Mg on creep properties

Fig. 9(a) shows typical creep curves of samples of Al−0.3Fe alloys with different Cu content as an example. During compressive creep deformation, the creep strain rapidly increases and the instant creep rate, $\dot{\varepsilon}$, decreases with increasing time, which can be defined as the primary creep stage. The primary stage ends when the $d\dot{\varepsilon}/dt \approx 0$. Subsequently, the creep deformation turns to a quasi-steady state, in which the creep rate, $\dot{\varepsilon}$, becomes more and less constant, which can be

defined as the second stage. The primary creep strain, ε_p, in the primary stage and the minimum creep rate, $\dot{\varepsilon}_m$, in the second stage are used here to characterize the creep properties during creep deformation. The primary creep strain, ε_p, is obtained by extrapolating the second creep curve linearly back to the zero time (Fig. 9(a), dotted line) according to literature,[22] while the minimum creep rate, $\dot{\varepsilon}_m$, is calculated as the average creep rate in the second stage (Fig. 9(b)).

Results of Fig. 9(a) show that the total creep strain greatly decreases due to the addition of Cu in 0.3Fe alloys, which decreases from 6.9% in Al−0.3Fe base alloy to 2.4% in Al−0.3Fe−0.29Cu alloy, indicating a general beneficial effect of the Cu addition on the creep properties. However, the minimum creep rate is almost unchanged with increasing Cu content (Fig. 9(b)), showing a mixed effect of the Cu addition on the creep properties. To clearly reveal the Cu effect, the primary creep stain, ε_p, and the minimum creep rate, $\dot{\varepsilon}_m$, in all three alloys (Al−0.3Fe, Al−0.5Fe and Al−0.7Fe) have been calculated and the results are shown in Fig. 10. It can be observed that ε_p is significantly decreased with increasing Cu content at a given Fe level (Fig. 10(a)). For instance, with increasing Cu content from 0% to 0.29%, the ε_p decreases from 3.82% to 0.43% in Al−0.3Fe alloys (89% reduction), from 1.25% to 0.22% in Al−0.5Fe alloys (82% reduction), and from 0.71% to 0.15% in Al−0.7Fe alloys (79% reduction), respectively. On the other hand, the addition of Cu has almost no influence on $\dot{\varepsilon}_m$ in all studied Fe contents (Fig. 10(b)). For example, the $\dot{\varepsilon}_m$ keeps almost constant at $8.1 \times 10^{-8}\,s^{-1}$ with 0.3Fe alloys and $5.5 \times 10^{-9}\,s^{-1}$ with 0.7Fe alloys, independent from the increase of Cu from 0% to 0.29%. It is evident that minor

Cu addition shows a beneficial effect to the creep properties mainly in controlling the creep deformation in the primary stage. However, it has a negligible effect on the minimum creep rate in the second creep stage.

It is worth mentioning that the benefit of Cu in the primary creep stage is decreased with increasing Fe content in the base alloys (Fig. 10(a)), which can be attributed to the increasing fine Fe-rich dispersoids and small subgrains acting as strong barriers to the dislocation movements during creep deformation from higher Fe content alloys.[20] Therefore, it is suggested that Cu addition would be more effective in increasing the creep property in low Fe content alloys.

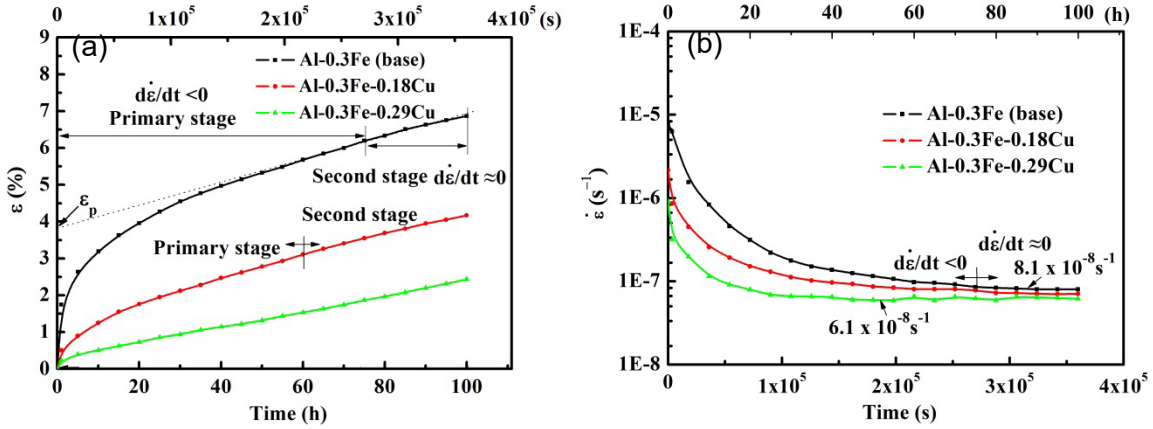

Fig. 9 Typical compressive creep curves of Al−0.3Fe alloys with different Cu content, tested at 100 °C and applied load of 69 MPa: (a) creep strain (ε) and (b) instantaneous creep rate ($\dot{\boldsymbol{\varepsilon}}$).

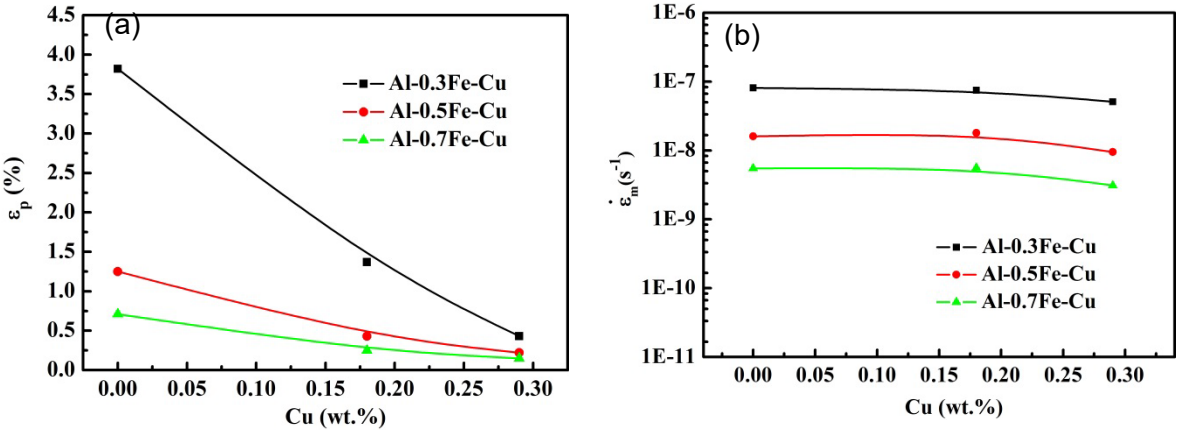

Fig. 10 Evolution of the primary creep strain (ε_p) (a) and minimum creep rate ($\dot{\boldsymbol{\varepsilon}}_{\boldsymbol{m}}$) (b) as a function of Cu content.

To illustrate the influence of Mg addition, the typical creep curves of samples of Al−0.3Fe−0.18Cu alloys with different amounts of Mg are shown in Fig. 11. Both total creep strain and minimum creep rate considerably decreased with increasing Mg content. The evolution of the primary creep stain ε_p and the minimum creep rate $\dot{\varepsilon}_m$ as a function of Mg content in three alloys (Al−0.3Fe−0.18Cu, Al−0.5Fe−0.18Cu and Al−0.7Fe−0.18Cu) is shown in Fig. 12. Similar to the Cu addition, the primary creep strain ε_p was greatly reduced with the additions of Mg (Fig. 12(a)). For example, with Mg increasing from 0% to 0.1%, the ε_p greatly decreases from 1.37% to 0.09% in Al−0.3Fe−0.18Cu alloys (93% reduction), from 0.43% to 0.07% in Al−0.5Fe−0.18Cu alloys (84% reduction) and from 0.25% to 0.05% in Al−0.7Fe−0.18Cu alloys (80% reduction), respectively. However, in contrast to the Cu addition, the $\dot{\varepsilon}_m$ was significantly reduced with Mg addition at all studied Fe contents. As shown in Fig. 12(b), with Mg increasing from 0% to 0.1%, $\dot{\varepsilon}_m$ noticeably decreased from $7.5 \times 10^{-8}\,s^{-1}$ to $4.8 \times 10^{-10}\,s^{-1}$ in Al−0.3Fe-0.18Cu alloys (99%

reduction), from 1.8 × 10^{-8} s^{-1} to 2.8 × 10^{-10} s^{-1} in Al−0.5Fe-0.18Cu alloys (98% reduction), and further from 5.6 × 10^{-9} s^{-1} to 2.1 × 10^{-10} s^{-1} in Al−0.7Fe-0.18Cu alloys (96% reduction), respectively. It can clearly be observed that minor Mg addition can greatly decrease both ε_p and $\dot{\varepsilon}_m$ and therefore has a great potential to enhance the creep properties, both in the primary stage and secondary stage of the creep deformation.

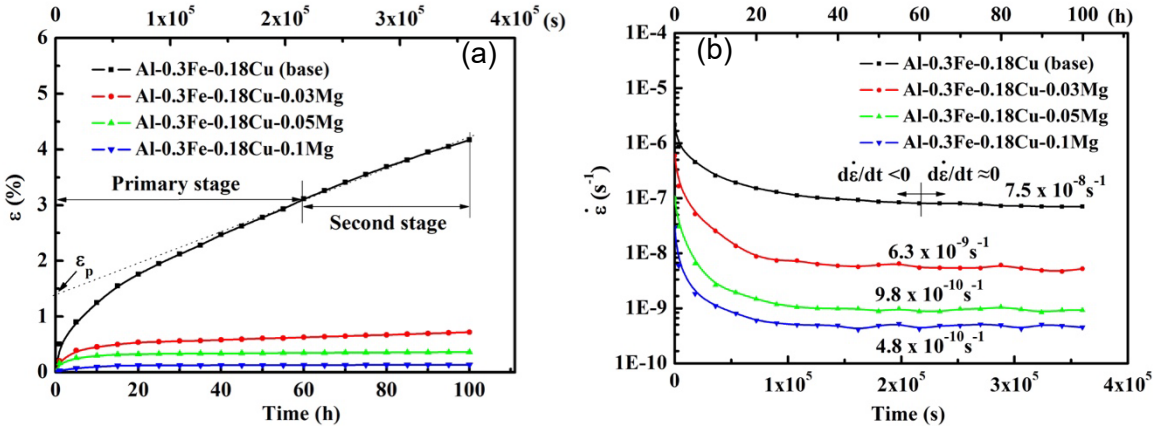

Fig. 11 Typical compressive creep curves of Al−0.3Fe−0.18Cu alloys with different Mg content, tested at 100 °C and applied load of 69 MPa: (a) creep strain (ε) and (b) instantaneous creep rate ($\dot{\boldsymbol{\varepsilon}}$).

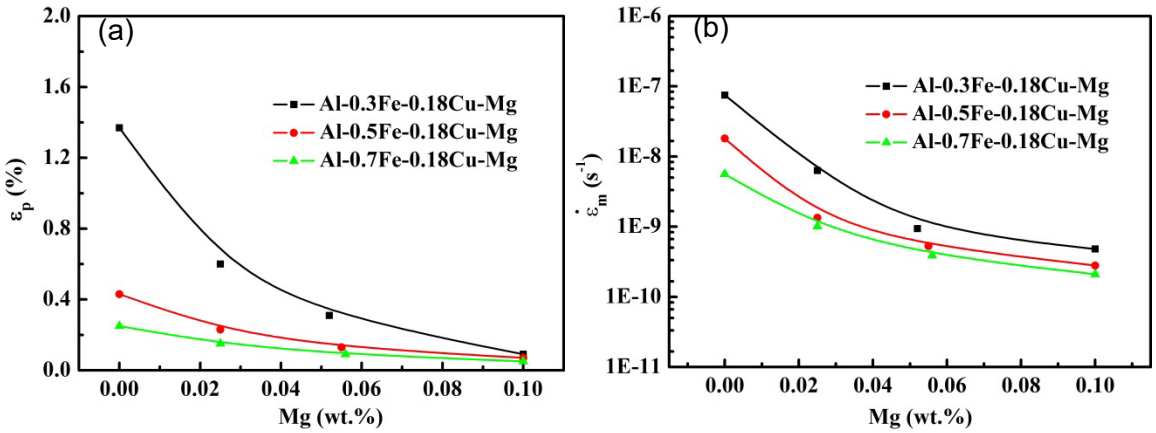

Fig. 12 Evolution of the primary creep strain (ε_p) (a) and minimum creep rate ($\dot{\boldsymbol{\varepsilon}}_{\boldsymbol{m}}$) (b) as a function of Mg content.

In the base alloys free of Cu and Mg, the creep properties are only dependent on the amount of Fe-rich intermetallic dispersion particles, which is in return controlled by Fe content in the alloys (Fig. 1). This is because only the Fe-containing intermetallic dispersion particles can act as barriers to dislocation movement during creep deformation in the base alloys. Higher Fe content and more Fe-containing intermetallic dispersion particles leads to better the creep properties (Figs. 10 and 12). With additions of minor Cu and Mg as solute atoms in the aluminum matrix, the creep properties (both ε_p and $\dot{\varepsilon}_m$) are significantly changed. For example, with additions of 0.29% Cu (Fig. 10(a)) or of 0.1%Mg (Fig. 12(a)) in Al-0.3Fe alloys, the ε_p remarkably decreased and approached the same value as the Al-0.7%Fe alloys. However, Cu and Mg influence the creep properties differently. Cu has a benefit principally on the primary stage (Figs. 9 and 10), while Mg can have positive impacts on both the primary and second stage of the creep deformation (Figs. 11 and 12). The different contributions of Cu and Mg on creep properties, can be derived

from the various behaviors of Cu and Mg. Firstly, work hardening is the principle controlling mechanism on the primary stage of creep deformation,[23] which is largely related to the solid solution levels that increase the work hardening ability of the material.[20] Therefore, the primary creep strain was greatly reduced with increasing amounts of Cu and Mg solutes. In addition, the subgrain size decreases with Cu addition (Fig. 3), which can retard the dislocation movement then further decrease the primary creep strain.

Secondly, the second stage of creep deformation is controlled by the glide and climb of dislocations in all studied alloys.[24] Hence, the creep properties can be influenced by the factors that can have an effect on the dislocation movements. It is reported that the interaction between dislocations and Cu solute atmosphere is low,[25,26] which is the likely reason for the negligible change in the minimum creep rate from Cu. On the other hand, the interaction of Mg with dislocations is stronger than Cu due to the higher atomic misfit with the aluminum matrix,[18,27] resulting in a possible increase in creep resistance in the second stage. Moreover, there is a strong tendency for Mg to form clusters with other elements[7,28] due to its much higher diffusivity (1.4×10^{-22} m^2/s vs 6.3×10^{-24} m^2/s of Cu at 100 °C[19,20]), which could lower the stacking fault energy, provide greater obstacles to dislocation glide and make intersections more difficult, leading to the further decrease of the minimum creep rate.[12,13,29,30] The formation of Mg clusters has been confirmed by using 3D atom probe tomography techniques,[12,13] resulting in a significant increase in the strength and a decrease in the minimum creep rate of aluminum alloys.

The creep is a relatively slow but time-dependent continuous deformation process. In the aspect of the creep resistance of materials, the improvement in the primary stage of the creep deformation (reducing the primary creep stain, ε_p) is mainly related to the short-term creep resistance. The decrease of the minimum creep rate, $\dot{\varepsilon}_m$, in the second stage of the creep deformation has a major contribution to the long-term creep resistance. As shown in Figs. 9 and 10, the minor Cu addition can only reduce ε_p but has negligible effect on $\dot{\varepsilon}_m$; hence, the beneficial effect of Cu in 8xxx alloys is limited to the short-term creep resistance. On the other hand, the minor Mg addition is highly effective in increasing both short-term and long-term creep resistances by simultaneously reducing ε_p and $\dot{\varepsilon}_m$. Therefore, minor alloying with Mg is more promising than Cu in terms of the small quantity required to enhance the creep resistance in 8xxx conductor alloys effectively while minimizing the impact on the electrical conductivity.

4. Conclusions

1. The addition of Cu promotes the retardation of the dynamic recovery, leading to a finer subgrain size. However, little change on the microstructure has been observed with the addition of Mg.

2. Additions of Cu and Mg reasonably increase the UTS but slightly decrease EC. The effects of Cu, Mg and Fe on the UTS and EC were quantitatively evaluated, providing a useful tool to predict the mechanical strength and electrical conductivity in 8xxx aluminum conductor alloys. With established UTS and EC profiles as a function of alloying elements (Cu, Mg and Fe), different combinations of UTS and EC could be obtained to fulfill various design requirements for

specific applications.

3. The minor addition of Cu remarkably decreases the primary creep stain but shows negligible effect on the minimum creep rate, leading to a beneficial effect on the short-term creep resistance but no advantage to the creep resistance under the long-term creep process.

4. The minor addition of Mg greatly reduces both primary creep strain and minimum creep rate, resulting in a significant and effective improvement on the creep resistance of 8xxx aluminum conductor alloys.

Acknowledgments

The authors would like to acknowledge financial support from Natural Science and Engineering Research Council of Canada (NSERC) and Rio Tinto through the NSERC Industrial Research Chair in Metallurgy of Aluminum Transformation at the University of Quebec at Chicoutimi.

References

1. O. Engler, G. Laptyeva and N. Wang: Impact of homogenization on microchemistry and recrystallization of the Al-Fe-Mn alloy AA 8006. *Mater. Char.* **79**, 60 (2013).

2. L. Pan, F. Breton, F. A. Mirza, K. Liu, and X.G. Chen: Effect of Fe-rich particles and solutes on creep behavior of 8xxx alloys. *Mater. Sci. Tech.* 2016, online published, http://dx.doi.org/10.1080/02670836.2016.1258156, 2016.11.18 (the date of access)

3. H.J. Mcqueen, E.H. Chia and E.A. Starke: Fe-particle-stabilized aluminum conductors. *JOM* **38**(4), 19 (1986).

4. A. Mamala and W. Sciezor: Evaluation of the effect of selected alloying elements on the mechanical and electrical aluminium properties. *Arch. Metall. Mater.* **59**(1), 413 (2014).

5. M.Y. Murashkin, I. Sabirov, X. Sauvage and R.Z. Valiev: Nanostructured Al and Cu alloys with superior strength and electrical conductivity. *J Mater Sci.* **51**(1), 33 (2016).

6. E.A. Marquis, D.N. Seidman and D.C. Dunand: Effect of Mg addition on the creep and yield behavior of an Al-Sc alloy. *Acta Mater.* **51**(16), 4751 (2003).

7. O. Ryen, O. Nijs, E. Sjolander, B. Holmedal, H.E. Ekstrom and E. Nes: Strengthening mechanisms in solid solution aluminum alloys. *Metall. Mater. Trans. A.* **37**(6), 1999 (2006).

8. R.A. Karnesky, L. Meng and D.C. Dunand: Strengthening mechanisms in aluminum containing coherent Al_3Sc precipitates and incoherent Al_2O_3 dispersoids. *Acta Mater.* **55**(4), 1299 (2007).

9. M.F. Ashby, H. Shercliff and D. Cebon: Materials: engineering, science, processing and design, 1st ed. (Elsevier Butterworth-Heinemann, Burlington, MA, USA, 2007), p. 514.

10. P.K. Chaudhury and F.A. Mohamed: Creep characteristics of an Al-2wt-percent-Cu alloy in the solid-solution range. *Mater. Sci. Eng., A* **101**, 13 (1988).

11. N.N. Du, Y. Qi, P.E. Krajewski and A.F. Bower: The effect of solute atoms on aluminum grain boundary sliding at elevated temperature. *Metall. Mater. Trans. A* **42**(3), 651 (2011).

12. R.N. Lumley, A.J. Morton and I.J. Polmear: Enhanced creep performance in an Al-Cu-Mg-Ag alloy through underageing. *Acta Mater.* **50**(14), 3597 (2002).

13. X. Sauvage, N. Enikeev, R. Valiev, Y. Nasedkina and M. Murashkin: Atomic-scale analysis of the segregation and precipitation mechanisms in a severely deformed Al-Mg alloy. *Acta Mater.* **72**, 125 (2014).

14. G.H. Reynolds, F.V. Lenel and G.S. Ansell: The effect of solute additions on the steady-state creep behavior of dispersion-strengthened aluminum. *Metall. Mater.Trans. B* **2**(11), 3027 (1971).

15. M. Kato: Grain boundary sliding in high-purity aluminium bicrystal and Al-Cu solid solution bicrystal during plastic deformation. *Trans. Jap. Ins. Met.* **10**(3), 215 (1969).

16. C.J. Shi, W.M. Mao and X.G. Chen: Evolution of activation energy during hot deformation of AA7150 aluminum alloy. *Mater. Sci. Eng., A* **571**, 83 (2013).

17. L. Pan, K. Liu, F. Breton, and X. G. Chen: Effect of Fe on microstructure and properties of 8xxx aluminum conductor alloys. *J. Mater. Eng. Perform.* **25**(11), 1059 (2016)

18. M. Spittel and T. Spittel: Part 2: Non-ferrous alloys-light metal, 4th ed. (Springer, Berlin, Germany, 2011), p. 19-53.

19. G. Neumann and C. Tuijn: Self-diffusion and impurity diffusion in pure metals: handbook of experimental data, 1st ed. (Elservier Ltd, Amsterdam, Netherlands, 2009), p. 349.

20. M. Shakiba, N. Parson and X.G. Chen: Hot deformation behavior and rate-controlling mechanism in dilute Al-Fe-Si alloys with minor additions of Mn and Cu. *Mater. Sci. Eng., A* **636**, 572 (2015).

21. B. Raeisinia, W.J. Poole and D.J. Lloyd: Examination of precipitation in the aluminum alloy AA6111 using electrical resistivity measurements. *Mater. Sci. Eng., A* **420**(1-2), 245 (2006).

22.X.W. Wei, X.T. Zu and W.L. Zhou: Compressive creep behaviour of Mg-Li-Al alloy. *Mater. Sci. Tech.* **22**(6), 730 (2006).

23. F.R.N. Nabarro: The time constant of logarithmic creep and relaxation. *Mater. Sci. Eng., A* **309**, 227 (2001).

24. R.W. Westerlund: Effects of composition and fabrication practice on resistance to annealing and creep of aluminum conductor alloys. *Metall. Trans.* **5**(3), 667 (1974).

25. F.A. Mohamed: Incorporation of the suzuki and the fisher interactions in the analysis of creep-behavior of solid-solution alloys. *Mater. Sci. Eng., A* **61**(2), 149 (1983).

26. M.D. Halliday and C.J. Beevers: Some observations of grain-boundary sliding in aluminium bicrystals tested at constant strain rate and constant rate of stress increase. *J. Mater. Sci.* **6**(10), 1254 (1971).

27. R.I. Babicheva, S.V. Dmitriev, Y. Zhang, S.W. Kok, N. Srikanth, B. Liu and K. Zhou: Effect of grain boundary segregations of Fe, Co, Cu, Ti, Mg and Pb on small plastic deformation of nanocrystalline Al. *Comp. Mater. Sci.* **98**, 410 (2015).

28. I.A. Ovid'ko, A.G. Sheinerman and R.Z. Valiev: Mg segregations at and near deformation-distorted grain boundaries in ultrafine-grained Al-Mg alloys. *J. Mater. Sci.* **49**(19), 6682 (2014).

29. S.A. Mahmoud, K.H. Georgy, F.M. Mansy and R. Kamel: Effect of cold work on the mechanism controlling the high temperature creep in Al− 2 wt% Mg. *phy. stat. sol. (a).* **51**(1), 257 (1979).

30. X.Y. Liu, Q.L. Pan, X.L. Zhang, S.X. Liang, F. Gao, L.Y. Zheng and M.X. Li: Creep behavior and microstructural evolution of deformed Al-Cu-Mg-Ag heat resistant alloy. *Mater. Sci. Eng., A* **599**, 160 (2014).

Table

Table I Chemical compositions of the experimental alloys (wt. %)

Alloys	Fe	Cu	Mg	Si	Mn	Cr	Zn	Al
Al-0.3Fe (L00)	0.30	**0.01**	0.001	0.025	0.002	0.001	0.012	Bal.
Al-0.3Fe-0.18Cu (L20)	0.30	**0.18**	0.001	0.023	0.003	0.001	0.002	Bal.
Al-0.3Fe-0.29Cu (L30)	0.30	**0.29**	0.000	0.033	0.001	0.001	0.012	Bal.
Al-0.3Fe-0.18Cu-0.03Mg (L23)	0.30	0.18	**0.025**	0.031	0.002	0.001	0.012	Bal.
Al-0.3Fe-0.18Cu-0.05Mg (L25)	0.30	0.19	**0.052**	0.038	0.003	0.001	0.002	Bal.
Al-0.3Fe-0.18Cu-0.1Mg (L210)	0.30	0.18	**0.100**	0.049	0.002	0.001	0.012	Bal.
Al-0.5Fe (M00)	0.46	**0.01**	0.001	0.046	0.002	0.001	0.012	Bal.
Al-0.5Fe-0.18Cu (M20)	0.50	**0.18**	0.001	0.027	0.004	0.001	0.002	Bal.
Al-0.5Fe-0.29Cu (M30)	0.47	**0.29**	0.000	0.023	0.002	0.001	0.003	Bal.
Al-0.5Fe-0.18Cu-0.03Mg (M23)	0.46	0.18	**0.026**	0.051	0.002	0.001	0.013	Bal.
Al-0.5Fe-0.18Cu-0.05Mg (M25)	0.44	0.17	**0.055**	0.021	0.001	0.001	0.002	Bal.
Al-0.5Fe-0.18Cu-0.1Mg (M210)	0.47	0.18	**0.100**	0.049	0.002	0.001	0.012	Bal.
Al-0.7Fe (H00)	0.70	**0.01**	0.001	0.023	0.002	0.001	0.013	Bal.
Al-0.7Fe-0.18Cu (H20)	0.70	**0.19**	0.001	0.042	0.003	0.001	0.016	Bal.
Al-0.7Fe-0.29Cu (H30)	0.71	**0.29**	0.000	0.032	0.003	0.001	0.002	Bal.
Al-0.7Fe-0.18Cu-0.03Mg (H23)	0.69	0.18	**0.027**	0.052	0.002	0.001	0.013	Bal.
Al-0.7Fe0.18-Cu-0.05Mg (H25)	0.70	0.18	**0.056**	0.042	0.003	0.001	0.012	Bal.
Al-0.7Fe-0.18Cu-0.1Mg (H210)	0.72	0.18	**0.100**	0.051	0.002	0.001	0.013	Bal.

Figure captions

Fig. 2 Optical micrographs showing the particles distribution of the alloys: (a) Al−0.3Fe, (b) Al−0.3Fe−0.29Cu, (c) Al−0.7Fe, and (d) Al−0.7Fe−0.18Cu−0.1Mg, showing fine Fe-containing intermetallic particles distributed along the extrusion direction (ED).

Fig. 2 Orientation image mapping showing the extruded microstructure of the alloys: (a) Al−0.3Fe, (b) Al−0.3Fe−0.29Cu, (c) Al−0.7Fe, (d) Al−0.7Fe−0.18Cu−0.1Mg and (e) inversed pole figure coloring and extrusion direction (ED). Boundary misorientation indicated as follows: white lines 1−5°, blue lines: 5−15°, thin black lines: 15−30°, and thick black lines > 30°.

Fig. 3 The evolution of subgrain size with an increase of (a) Cu and (b) Mg content.

Fig. 4 Influence of alloying elements on electrical conductivity: (a) Cu and (b) Mg.

Fig. 5 Correlation between calculated and experimentally measured EC.

Fig. 6 Influence of individual alloying elements on UTS: (a) Cu, (b) Mg and (c) Fe with a linear relationship.

Fig. 7 Correlation between calculated and experimentally measured UTS.

Fig. 8 EC and UTS profile of the alloys with different Cu and Mg addition. Arrows show the increasing Cu and Mg additions to their corresponding regions.

Fig. 9 Typical compressive creep curves of Al−0.3Fe alloys with different Cu content, tested at 100 °C and applied load of 69 MPa: (a) creep strain (ε) and (b) instantaneous creep rate ($\dot{\boldsymbol{\varepsilon}}$).

Fig. 10 Evolution of the primary creep strain (ε_p) (a) and minimum creep rate ($\dot{\boldsymbol{\varepsilon}}_{\boldsymbol{m}}$) (b) as a function of Cu content.

Fig. 11 Typical compressive creep curves of Al−0.3Fe−0.18Cu alloys with different Mg content, tested at 100 °C and applied load of 69 MPa: (a) creep strain (ε) and (b) instantaneous creep rate ($\dot{\boldsymbol{\varepsilon}}$).

Fig. 12 Evolution of the primary creep strain (ε_p) (a) and minimum creep rate ($\dot{\boldsymbol{\varepsilon}}_{\boldsymbol{m}}$) (b) as a function of Mg content.